FINAL ACCEPTED VERSION

Core Doped $[(Cd_{1-x}Co_x)_{10}S_4(SPh)_{16}]^{4-}$ Clusters from a Self-Assembly Route

Jillian E. Denhardt and Kevin R. Kittilstved*

Department of Chemistry, University of Massachusetts Amherst, 710 N Pleasant St, Amherst, MA 01003

*email – kittilstved@chem.umass.edu

ABSTRACT: The incorporation of substitutional Co^{2+} impurities in $[Cd_{10}S_4(SPh)_{16}]^{4-}$ (Cd_{10}) molecular clusters prepared by self-assembly method where Na_2S is the sulfur precursor and a redox method where elemental S is the sulfur precursor is studied. The Co^{2+} ions provide unique spectroscopic and chemical handles to monitor dopant speciation during cluster formation as well as determine what role, if any, other cluster species play during Cd_{10} cluster formation. In contrast to the redox method that produces exclusively surface-exchanged Co:Cd_{10}, the preparation of Cd_{10} by the self-assembly method in the presence of Co^{2+} ions results in Co^{2+} incorporation at both the surface and core sites of the Cd_{10} cluster. Electrospray ionization mass spectrometry (ESI-MS) analysis of the dopant distribution for the self-assembly synthesis of Co^{2+}-doped Cd_{10} is consistent with a near-Poissonian distribution for all nominal dopant concentrations albeit with reduced actual Co^{2+} incorporation. At a nominal Co^{2+} concentration of 50% we observe incorporation of up to seven Co^{2+} ions within the Cd_{10} self-assembled cluster compared to a maximum of only four Co^{2+} dopants in the Cd_{10} redox clusters. The observation of up to seven Co^{2+} dopants must involve substitution of at least three core sites within the Cd_{10} cluster. Electronic absorption spectra of the Co^{2+} ligand field transition in the heavily Co:Cd_{10} clusters display clear deviation with the surface-doped Co^{2+}-doped Cd_{10} clusters prepared by the redox method. We hypothesize that the coordination of Co^{2+} and S^{2-} ions in solution prior to cluster formation, which is possible only with the self-assembly method, is critical to the doping of Co^{2+} ions within the Cd_{10} cores.

INTRODUCTION

Inorganic semiconductor nanoclusters have gained interest for their atomically precise sizes and well defined structures.[1,2] The class of molecular metal chalcogenide clusters can range in size from tens to hundreds of atoms within the core and up to ~2 nm in size. These clusters experience size-dependent changes of their electronic structures, including the observations that larger nanoclusters have some overlapping properties with colloidal nanocrystals.[3–6] These similarities make nanocluster molecules ideal structural and spectroscopic analogues to larger nanocrystals.[7,8] Developing synthetic methods for achieving a diverse range of cluster sizes has been challenging. Some previously synthesized examples of these molecular clusters of particular interest are the cadmium thiophenolate species including, $[Cd(SPh)_4]^{2-}$ (Cd_1), $[Cd_4(SPh)_{10}]^{2-}$ (Cd_4), $[Cd_{10}S_4(SPh)_{16}]^{4-}$ (Cd_{10}), $[Cd_8S(SPh)_{16}]^{2-}$ (Cd_8), $[Cd_{17}S_4(SPh)_{28}]^{2-}$ (Cd_{17}), and $[Cd_{32}S_{14}(SPh)_{36}(dmf)_4]$ (Cd_{32}).[9–13] Additionally, there have been many reports on the role of cluster species within the growth mechanism of quantum dots (QDs), in addition to the use of molecular clusters as precursors for further growth.[14–18] The use of molecular cluster precursors has also been promising for effectively doping QDs with transition metal ions.[19,20] With increasing evidence of clusters being metastable intermediates in the synthesis of colloidal semiconductor nanocrystals, the attention of many researchers has shifted to understanding the chemistry of these cluster species and related magic-size nanocrystals as they may be critical to controlling dopant distributions within nanocrystals and maintaining narrow size distributions.[21–25]

Our group has previously reported on the doping of Co^{2+} ions within pre-formed Cd_4, Cd_{10}, and Cd_{17} clusters.[26] One of the main conclusions of that study was the assignment of the rate-determining step for the metal ion exchange to the ligand interconversion rate of bridging and terminal thiophenolate ligands as evidenced by variable-temperature ^{1}H-NMR spectroscopy that decreased with increasing cluster nuclearity. Therefore, due to the rapid surface interconversion necessary for metal-ion exchange, the doping was fastest for Cd_4 with only one unique metal site compared to Cd_{10} and Cd_{17} clusters that have at least two unique metal sites and S^{2-} ions within the cluster cores.[26,27] The two unique cation sites in the Cd_{10} cluster are unevenly split into four surface sites with $(\mu\text{-SPh})_3(SPh)_1$ coordination and six core sites with $(\mu_3\text{-S})_2(\mu\text{-SPh})_2$ coordination. These "surface" and "core" sites are equivalent to the apex and edge sites of a T3-shaped supertetrahedral cluster,[28] respectively. We prefer the surface and core terms to emphasize the relative accessibility of these two distinct sites and for comparison to their larger nanocrystal analogs. Due to substitution primarily at surface sites from the cation exchange mechanism with pre-formed clusters, our group has developed alternative strategies to overcome this limitation in Cd_{10} and larger clusters by including dopants in the reaction solution prior to addition of the S^{2-} precursor. This method allowed us to selectively dope Mn^{2+} at both the core and surface sites within the Cd_{10} cluster, evidenced by the Mn^{2+}-centered photoluminescence (PL) and electrospray ionization mass spectrometry (ESI-MS).[29]

Herein, we demonstrate the Cd_{10} cluster can be prepared with up to seven Co^{2+} ions substituting Cd^{2+} sites confirmed by ESI-MS by a self-assembly method utilizing Na_2S as the S^{2-} source. In contrast, Cd_{10} clusters prepared by a redox method where SPh^- ligands of Cd_4 clusters in situ reduce S to S^{2-} can incorporate only up to four Co^{2+} ions per Cd_{10}. Furthermore, the ESI-MS intensities for a series of Co^{2+}-doped Cd_{10} (Co:Cd_{10}) product fragments with the general formula $[(Cd_{10-x}Co_x)S_4(SPh)_{14}]^{2-}$ prepared by the self-assembly method nearly follows Poissonian doping statistics based on the nominal mol fraction (x) despite the presence of two unique Cd^{2+}

sites within the Cd_{10} cluster as shown in Figure 1. Comparison of the Co^{2+} speciation in the self-assembled Cd_{10} (Co:Cd_{10}-SA) and the redox method (Co:Cd_{10}-R) allows us to explore the effect of dopant speciation on the electronic structures of Co^{2+} dopants located at the surface and core sites in the lattice and solution chemistry (cluster equilibria and dynamics) of the clusters. We propose that (1) decreasing Cd^{2+} to Co^{2+} ratio while maintaining the overall M^{2+} concentration and (2) allowing Co^{2+}-S^{2-} bonds to form through this self-assembly approach enables the substitution of Co^{2+} into the Cd_{10} cores. The ability to obtain high dopant concentrations in these Cd_{10} clusters provides an intriguing platform to explore their potential as true single-source precursors for further nanocluster, magic-sized cluster, and quantum dots with controlled dopant concentrations and distributions.

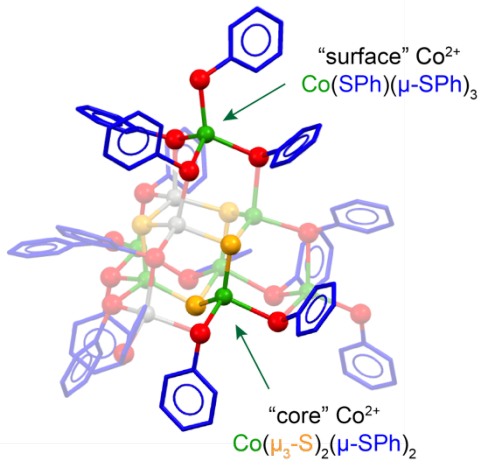

Figure 1. One possible representation of a heavily-doped $[(Cd_3Co_7)S_4(SPh)_{16}]^{4-}$ cluster with Co^{2+} substitution at both core and surface sites. Legend: Co^{2+} (green), Cd^{2+} (gray), S^{2-} (orange), and SPh^- (red with blue C_6H_5 rings). In this representation the Co^{2+} dopants are at every surface site (four total) and half of the core sites (three out of six).

MATERIALS AND METHODS

Chemicals. Cadmium nitrate tetrahydrate ($Cd(NO_3)_2{\cdot}4H_2O$, 99+% ACROS Organics), sodium sulfide nonahydrate ($Na_2S{\cdot}9H_2O$, 98%, Alfa Aesar), thiophenol (PhSH, 99%, ACROS Organics), cobalt nitrate hexahydrate ($Co(NO_3)_2{\cdot}6H_2O$, 99%, ACROS Organics), tetramethylammonium hydroxide pentahydrate ($TMAOH{\cdot}5H_2O$, 98%, ACROS Organics), anhydrous acetonitrile (CH_3CN, 99.9+%, ACROS Organic), anhydrous methanol (CH_3OH, 99.8%, ACROS Organics), triethylamine (Et_3N, 99%, Fisher), and elemental sulfur (S, ACROS Organics) were used without further purification. *Caution!* Thiophenol is extremely toxic and has an unpleasant odor. Handle with caution according to the material safety data sheet.

Redox Synthesis of $(NMe_4)_4[(Cd_{1-x}Co_x)_{10}S_4(SPh)_{16}]$ – referred to as Co:Cd_{10}-R. We have previously reported this synthesis that was adapted from others.[9,26] Briefly, $(NMe_4)_2[Cd_4(SPh)_{10}]$ (Cd_4) clusters were prepared by literature methods[9] and used in the preparation of Cd_{10} via a redox method under air free conditions in an N_2 filled glovebox. Elemental S powder (0.62 mmol) was added to the dissolved Cd_4 cluster (0.59 mmol) in 4 mL of CH_3CN. A yellow precipitate was formed and allowed to stir for 30 minutes, which resulted in a white precipitate. The solution was then heated to ~70 °C and CH_3CN was added until the precipitate dissolved completely and allowed to cool slowly to recrystallize the pure Cd_{10}. The solution remained undisturbed for 2 days, which formed small colorless crystals. At this point diethyl ether was added to the solution and allowed to sit for an additional day before vacuum filtering the powder Cd_{10} product and washing with CH_3OH. In the case of Co^{2+} doping, $Co(NO_3)_2{\cdot}6H_2O$ (10% nominal, 0.264 mmol, 0.0767 g) was dissolved in 1 mL of CH_3CN and added to the reaction solution after the dissolution of the Cd_{10} precipitate to facilitate a cation exchange reaction. At higher nominal dopant concentrations (30 and 50% Co^{2+}), the addition of M^{2+} shifts the cluster equilibria to yield $(NMe_4)_2[(Cd_{1-x}Co_x)_{17}S_4(SPh)_{28}]$ (see Figure S1 and Table S1).

Co:Cd_{10}-R was also synthesized from nominally 10% and 30% Co:Cd_4 precursors as a single source of both the Co^{2+} and Cd^{2+} ions. At 30% nominal Co^{2+} in the Co:Cd_4, however, the synthesis yields undesired $(NMe_4)_2[(Cd_{1-x}Co_x)_{17}S_4(SPh)_{28}](NMe_4)_2$ (Co:Cd_{17}) and $(NMe_4)_2[(Cd_{1-x}Co_x)_8S(SPh)_{16}]$ (Co:Cd_8) clusters, (see Figure S1 and Table S1).

The redox method proceeds by the following balanced reaction, $5[Cd_4(SPh)_{10}]^{2-} + 8S \rightarrow 2[Cd_{10}S_4(SPh)_{16}]^{4-} + 8PhSSPh + 2SPh^-$.

Self-Assembly Synthesis of $(NMe_4)_4[(Cd_{1-x}Co_x)_{10}S_4(SPh)_{16}]$ – referred to as Co:Cd_{10}-SA. In contrast to the redox method to prepare Cd_{10} involving the addition of elemental S to Cd_4, self-assembly cluster synthesis is adapted from our previous report and that of Lee et al, with the exception of Co^{2+} addition.[12,29] All reactions were performed under air free conditions in an N_2 filled glovebox. To a stirring solution of PhSH (5.20 mmol, 0.53 mL) and Et_3N (5.20 mmol, 0.73 mL) in CH_3CN (3.5 mL), a metal ion solution of $Cd(NO_3)_2{\cdot}4H_2O$ and $Co(NO_3)_2{\cdot}6H_2O$ (2.38 mmol total in 2 mL of CH_3CN) was added dropwise. A solution of $Na_2S{\cdot}9H_2O$ (1.20 mmol in 5 mL CH_3OH) was then added dropwise followed directly by the addition of TMAOH (1.17 mmol in 1 mL CH_3OH) that immediately forms a pale yellow or green precipitate. After 24 hours of stirring, the mixture was vacuum filtered and washed with excess CH_3OH. The nominal dopant amount is dictated by the ratio of cadmium to cobalt used, which equals a total amount of 2.38 mmol. For undoped clusters, $Co(NO_3)_2{\cdot}6H_2O$ would be excluded and 2.38 mmol of $Cd(NO_3)_2{\cdot}4H_2O$ would be solely used whereas for 10% nominal Co^{2+} doping, 0.238 mmol of $Co(NO_3)_2{\cdot}6H_2O$ and 2.14 mmol $Cd(NO_3)_2{\cdot}4H_2O$ were dissolved into the same solution by CH_3CN.

The balanced reaction describing the self-assembly reaction is given by, $10Cd^{2+} + 16SPh^- + 4S^{2-} \rightarrow [Cd_{10}S_4(SPh)_{16}]^{4-}$.

Physical Characterization. Room temperature absorption was collected with a Cary 50. The Cd_{10} clusters were dissolved in anhydrous CH_3CN in the glovebox. High-resolution electrospray ionization mass spectra (ESI–MS) were collected in negative ion mode with a cone voltage of −10 V unless stated otherwise with a Bruker Micro-TOF-II. The flow rate of samples was set to 3 μL/min for ESI-MS. Analysis of the mass spectra was performed using mMass software. Powder X-ray diffraction (XRD) patterns were collected at room temperature using a Bragg-Brentano configuration with Cu K-α source (with cross-beam optics and D/Tex 250 Ultra 1D Si strip detector) of dried samples on "zero-background" sample holders (Rigaku SmartLab SE Diffraction System).

RESULTS AND DISCUSSION

Figure 2 shows the negative-mode ESI-MS spectra collected at −10 V of the $(Cd_{1-x}Co_x)_{10}$-SA clusters prepared with increasing nominal dopant concentrations up to $x = 0.5$, but constant total

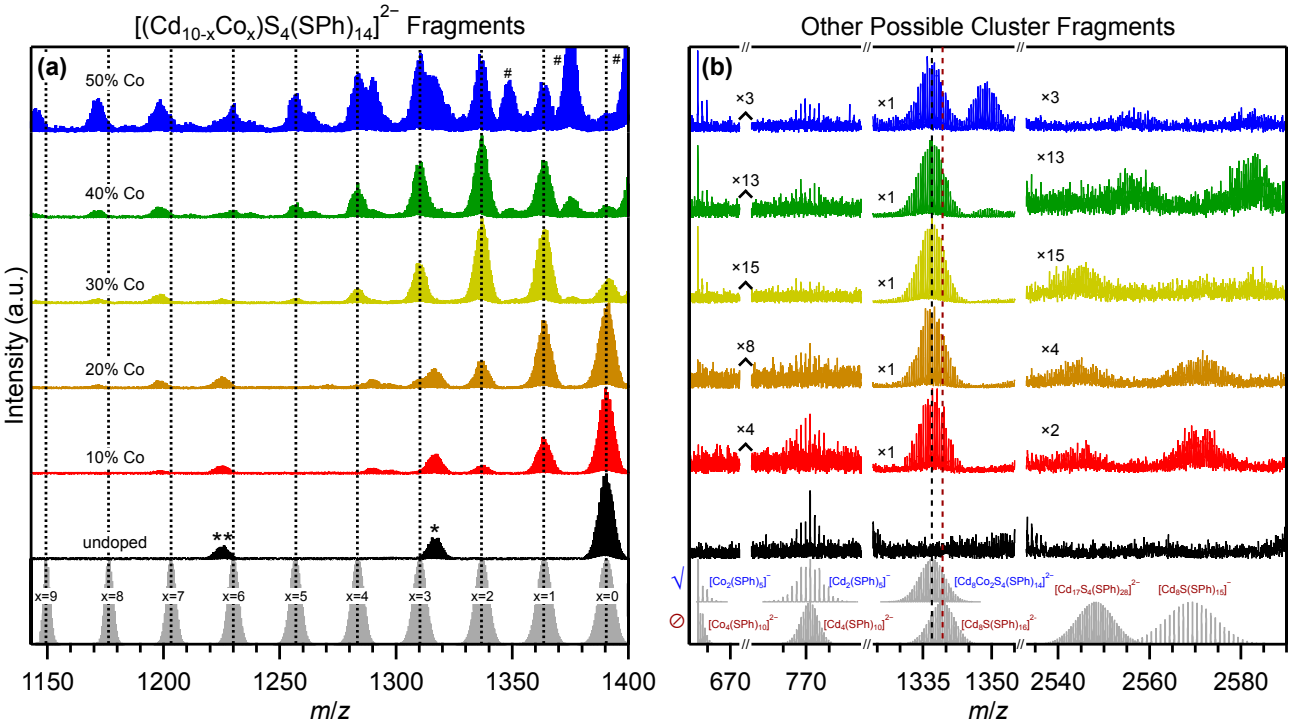

Figure 2. ESI-MS spectra of the $(Cd_{1-x}Co_x)_{10}$-SA clusters with increasing nominal dopant concentration from x = 0 to x = 0.5 in the region of (a) the $[Cd_{10-x}Co_xS_4(SPh)_{14}]^{2-}$ fragments and (b) the regions where other possible cluster fragments are expected (Co_4, Cd_4, Cd_8, and Cd_{17}). The identified spectra are either observed (identified by the row with the √) or not observed (Ø). The spectra at the bottom of (a) and (b) are simulated fragments with charges of $z = -1$ or -2 as stated in the figure. In (a) the features at 1320 (*) and 1224 (**) are $(NMe_4)[Cd_9S_4(SPh)_{13}]^{2-}$ and $[Cd_9S_4(SPh)_{12}]^{2-}$ product fragments from the Cd_{10} cluster, respectively. In (a) the features at m/z 1401, 1375, and 1348 (#) are $(NMe_4)[Cd_{10-x}Co_xS_4(SPh)_{15}]^{2-}$ product fragments for x= 3, 4, and 5, respectively. The full ESI-MS spectra and list of peak assignments can be found in Figure S2 and Table S2. The tick spacing for the x-axes in (b) is 5 m/z units.

cation content ([Co]+[Cd]=2.38 mmol). Figure 2(a) displays just the spectral range of the majority product fragment of Cd_{10} that is missing two SPh^- ligands at m/z 1391, $[Cd_{10}S_4(SPh)_{14}]^{2-}$. Additional Cd_{10} product fragments are observed at m/z 1224 and 1320 that match well to $[Cd_9S_4(SPh)_{12}]^{2-}$ and $(NMe_4)[Cd_9S_4(SPh)_{13}]^{2-}$, respectively. With increasing nominal Co^{2+} concentration, two changes are observed with this $[(Cd_{1-x}Co_x)_{10}S_4(SPh)_{14}]^{2-}$ product fragment. First, the relative intensity of the undoped Cd_{10} fragment at m/z 1391 decreases with increasing nominal Co^{2+} concentration. Second, new peaks appear at integer multiples of half the mass difference between Co and Cd ($\delta m \approx -53.5$ amu; $z = 2$; $\delta m/z \approx -26.7$). These lower m/z peaks associated with Co^{2+} substitution in Cd_{10} gain intensity and redistribute towards lower m/z values with increasing nominal Co^{2+} concentration. For example, the ESI-MS data for the sample prepared from a solution with a nominal concentration of 10% Co^{2+} displays a similar fragmentation pattern as the undoped Cd_{10} cluster but containing additional fragments at m/z ~1364 and ~1337 that originate from singly-doped and doubly-doped Cd_{10} precursor clusters, respectively. The relative intensities originating from fragments containing more than 2 Co^{2+} ions also increase with increasing nominal x and the most intense fragment shifts from the undoped Cd_{10} fragment to fragments containing up to 3 Co^{2+} ions. At the maximum nominal doping level of 50% studied, we can observe fragments containing up to 7 Co^{2+} ions within this Cd_{10} product fragment, $[Cd_3Co_7(SPh)_{14}]^{2-}$. These results indicate that the majority of Cd_{10} clusters contain at least one Co^{2+} dopant when the nominal doping concentration is ≥ 20%. While we cannot distinguish the exact dopant location from ESI-MS, we know that there must be a mixture of Co^{2+} ions within the core and surface sites in the Cd_{10} clusters with at least 5 Co^{2+} ions.

Figure 2b shows different regions of the ESI mass spectra where other common $z = -1$ and -2 fragments originating from other clusters such as Cd_4, Co_4, Cd_8, or Cd_{17} have been reported.[9,10,12,30,31] The absence of any additional clusters in Figure 2b is consistent with Co:Cd_{10} being the primary product of the Co:Cd_{10}-SA synthesis with this fixed reaction stoichiometry (see Table S2). We do observe product fragments associated with $[Cd_2(SPh)_5]^{1-}$ and $[Co_2(SPh)_5]^{1-}$, however, these are also common fragments in the ESI-MS of $[(Cd_{1-x}Co_x)_4(SPh)_{10}]^{2-}$ clusters. The absence of Cd_4 and Cd_8 fragments with Co^{2+} replacing Cd^{2+} suggests that Cd_{10} formation by the SA method is not affected by the presence of Co^{2+} instead of Cd^{2+}. We previously observed[29] additional Cd_4 and Cd_8 based fragments by ESI-MS in aliquots removed from the reaction mixture after *sub*-stoichiometric addition of S^{2-}. These intermediates were similarly observed in the synthesis of the Co^{2+} doped Cd_{10} cluster by ESI-MS, however the Cd_8 fragments decreased in relative intensity as the Cd_{10} fragments increased in relative intensity (see Figure S3). Additionally, we observe Co:Cd_4 as a reaction intermediate and do not observe the formation of the Co_4 cluster until all of the S^{2-} has

been added, indicating this cluster does not inhibit the formation of the Co:Cd_{10}.

The fragmentation of the more heavily doped Co:Cd_{10}-SA clusters was also studied by ESI-MS at higher cone voltages up to −80 V (see Figure S4 and S5). The expected increase in the degree of cluster fragmentation resulted in the observation of negatively-charged product fragments with the general formula $[(Cd_{7-x}Co_x)S_4(SPh)_8]^{2-}$. This fragment is comprised of all six core metal sites and a lone surface cation. At 50% nominal doping, we clearly observe substitution of up to two Co^{2+} ions in this heptanuclear product fragment that must include at least one Co^{2+} dopant at a core site.

If the doping process of Co^{2+} into the Cd_{10} cluster was stochastic, then the distribution of dopant ions per cluster should be Poissonian according to eq 1.[31]

$$P(n) = \frac{(xN)^n e^{-xN}}{n!} \quad (1)$$

where x is the dopant mol fraction defined by $x = [Co^{2+}]/([Co^{2+}]+[Cd^{2+}])$, N is the number of cation sites per cluster, and n is the actual number of dopants per cluster. Analysis of the ESI-MS data in Figure 2a produced relative intensities of the individual fragments for Co:Cd_{10}-SA clusters with x_{nom} = 0.1, 0.3, and 0.5 are shown in Figure 3 (see Figure S6 for all nominal x values). Assuming that all Co^{2+}:Cd_{10}-based fragments have equal probabilities of being detected, then we immediately see that the Co^{2+} incorporation in the clusters increases with nominal x. Simulated Poissonian distributions where x in eq 1 is equal to x_{nom} does not agree well with the data shown in Figure 3. However, allowing x in eq 1 to be a fitting parameter results in much better agreement to the experimental data. The restriction of the experimental fragments containing at most 5 Co^{2+} ions was necessary based on the diminishing spectral intensity and overlapping fragments making deconvolution of the relative intensities difficult. The overall trend that the calculated mol fraction, x, in the Co:Cd_{10}-SA clusters is lower than the nominal mol fraction, x_{nom}, for all samples and suggests that a chemical barrier (kinetic or thermodynamic) results in Co^{2+} being excluded from the Cd_{10} cluster during assembly. However, the fact that clusters with >4 Co^{2+} are observed with relative intensities that agree with the Poissonian distribution shown in Figure 3b further suggests no significant barrier exists between Co^{2+} substitution at a surface versus core site in the lattice prepared by this SA method. Previous observations demonstrated a significant barrier to core doping when either Mn^{2+} or Co^{2+} ions are added to pre-formed Cd_{10} clusters where doping is only active through a metal ion exchange mechanism.[26,29]

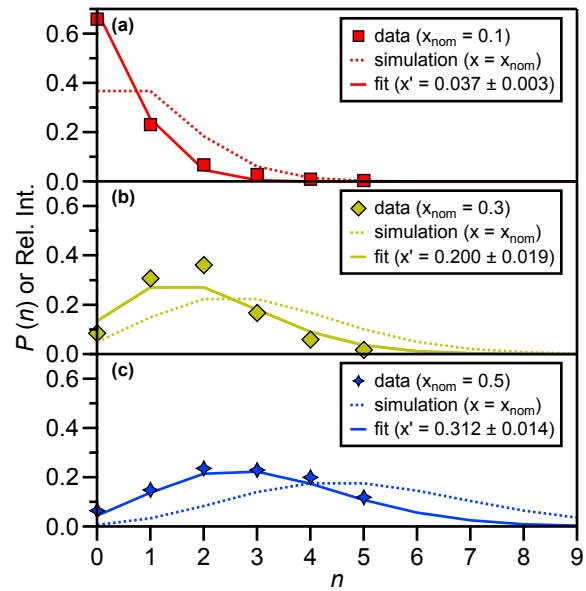

Figure 3. Relative intensities from the ESI-MS data shown in Figure 2a for the fragments with the general formula $[(Cd_{10-n}Co_n)S_4(SPh)_{14}]^{2-}$ where n is the actual number of Co^{2+} dopants per cluster and spans values between 0 and 5 (filled symbols) for $(Cd_{1-x}Co_x)_{10}$-SA clusters prepared with nominal x = (a) 0.1, (b) 0.3, and (c) 0.5. In each panel, the simulated Poissonian distribution when $x = x_{nom}$ in eq 1 is plotted as a dotted line, and the best fit of the data where x is the lone fitting parameter of eq 1 is shown as a solid line.

Electronic absorption spectroscopy was used as a dopant-specific probe of the Co^{2+} speciation within the Cd_{10} clusters as the Co^{2+}-centered excited states have been shown previously to be very sensitive to the unique ligand field environments imposed by core versus surface sites.[32–35] Figure 4a displays the electronic absorption spectra of the Co:Cd_{10}-SA clusters with increasing dopant concentration. The spectra of all pure and doped Cd_{10} clusters are dominated by an intense feature in the UV region that is assigned to the ligand-to-metal charge transfer of the host cluster and intraligand $\pi \rightarrow \pi^*$ of the thiophenolate ligands.[26] At low Co^{2+} doping levels a weak, structured absorption feature in the visible region between 650 nm – 800 nm appears. This visible absorption band is the $^4A_2 \rightarrow {}^4T_1(P)$ transition from Co^{2+} ions in a pseudo-tetrahedral ligand field. As the dopant concentration increases in the Co:Cd_{10} clusters shown in Figure 4a, the absorption features throughout the visible region broaden and become fairly unresolved at x = 0.5. This broadening is caused by inhomogeneous broadening that originates from a combination of Co^{2+} dopants occupying multiple sites within the cluster and structural distortions due to Co^{2+} ions occupying more and more Cd^{2+} sites of the Cd_{10} cluster.

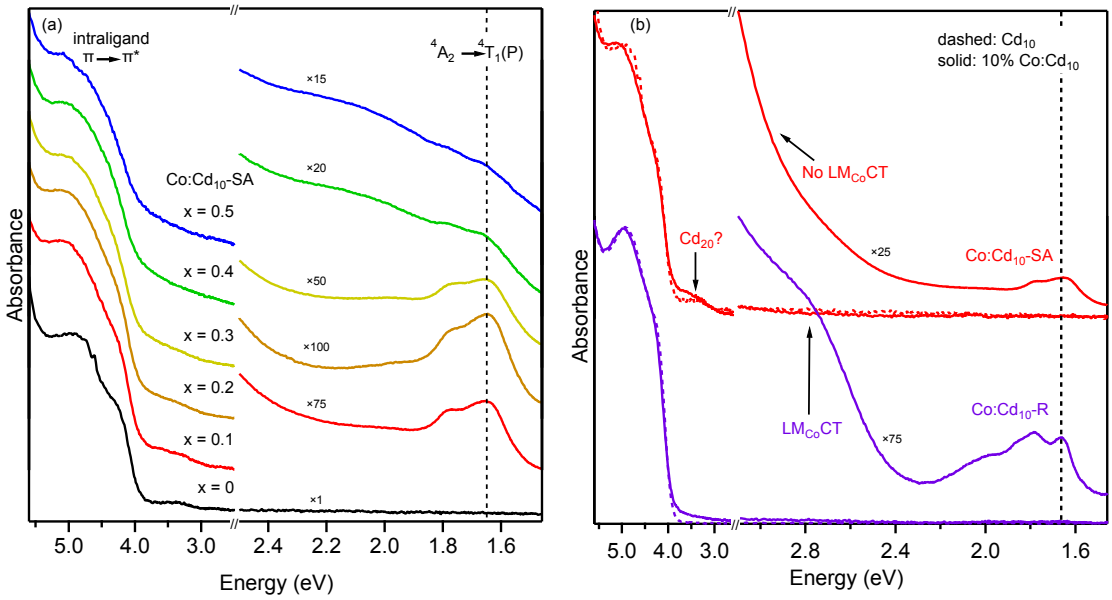

Figure 4. (a) Electronic absorption spectra of $(Cd_{1-x}Co_x)_{10}$-SA with increasing nominal x from 0 to 0.5. (b) Comparison of the spectra of cluster with the $(Cd_{0.9}Co_{0.1})_{10}$-R. Note that different regions of the spectra may be scaled as indicated in the figure by the multiplication symbol, ×.

We previously reported the absorption spectrum of $Co:Cd_{10}$ prepared by first forming Cd_{10} clusters by the redox method and then adding Co^{2+} ions producing $Co:Cd_{10}$-R clusters where metal ion exchange occurs only at the cluster surface.[26] Figure 4b compares the electronic absorption spectra of Cd_{10}-SA, 10% $Co:Cd_{10}$-SA, Cd_{10}-R and 10% $Co:Cd_{10}$-R. The absorption bands in the UV region of pure and 10% $Co:Cd_{10}$ clusters are similar with one exception. As seen in Figure 4b, the pure and 10% $Co:Cd_{10}$-SA spectra display a weaker transition around 360 nm that becomes less resolved with increasing Co^{2+} content (see Figure 4a). This absorption in the near-UV region is reminiscent of the exciton-like absorption observed for the sulfide core of the Cd_{17} or larger $[Cd_{20}S_{13}(SPh)_{22}]^{8-}$ cluster,[26,36] however, no evidence supporting the Cd_{20} cluster has been observed by ESI-MS techniques. In addition, the relative absorbance of the 360 nm transition to the intraligand transition is not constant from batch to batch, suggesting that two unique species are present in solution with different concentrations (see Figure S7). There is also no ligand-to-metal charge-transfer ($LM_{Co}CT$) transition in the $Co:Cd_{10}$-SA absorption spectrum at ~450 nm that is observed in the spectrum of $Co:Cd_{10}$-R.[26] This further supports the tentative assignment of this sub-bandgap feature to the formation of the Cd_{20} cluster, as large clusters and small QDs with exciton-like transitions are known to occlude this $LM_{Co}CT$.[37]

Closer inspection of the $^4A_2 \rightarrow {}^4T_1(P)$ transition shown in Figure 5a reveals subtle variations in the energies and relative intensities of the spin-orbit split $^4T_1(P)$ excited state between the $Co:Cd_{10}$-SA and $Co:Cd_{10}$-R clusters compared to the colloidal Co:CdS nanocrystals.[35] We attribute these variations to changes in the average ligand field environment of the Co^{2+} dopants between the clusters. Specifically, the data in Figure 5a supports the majority of Co^{2+} dopants occupy either surface or core sites in the $Co:Cd_{10}$-SA cluster whereas the Co^{2+} dopants are only occupying surface sites in the $Co:Cd_{10}$-R cluster. The ligand-field splitting ($10Dq$) and Racah (B) parameters for Co^{2+} ions with 4 SPh^- (Co_1), 1 terminal and 3 μ-SPh^- (Co_4), or 4 μ_4-S^{2-} (Co:CdS) ligand field environments are given in Table 1. These energies differ significantly as shown in the Co^{2+} Tanabe-Sugano diagram in Figure 5b where the x-axis is the ligand field strength ($10Dq/B$) imposed by these lattices. Both terminal and μ-SPh^- ligands have stronger ligand fields compared to μ_4-S^{2-}. Thus, Co^{2+} coordinated to μ_3-S^{2-} and μ-SPh^- ligands within the Cd_{10} core should cause this transition to redshift in comparison to strictly surface SPh^- coordination.[32–34] The bandshape of the $^4T_1(P)$ transition differs vastly among the coordination environments of Co^{2+} in Co_1, Co_4, and Co:CdS nanocrystals with increased intensity in the highest energy band observed only in the Co_4 cluster and is attributed to bridging SPh^- ligands.[32,35,38] The observation of the overall slightly red-shifted $^4T_1(P)$ transition for the 10% $Co:Cd_{10}$-SA compared to 10% $Co:Cd_{10}$-R in Figure 5a suggests the Co^{2+} is coordinated to sulfide ligands in the core, which provide a weaker ligand field than either terminal or bridging thiophenolate ligands. The $^4T_1(P)$ absorption for $Co:Cd_{10}$-SA is qualitatively more similar to the Co:CdS transition[35] in terms of band shape than $Co:Cd_{10}$-R.

Table 1. Experimental Ligand Field Parameters for Tetrahedral Co^{2+} with SPh^- and S^{2-} Ligands

Lattice	$\lvert 10Dq \rvert$	B_c	β^a	ref
$[Co(SPh)_4]^{2-}$, Co_1	4030	619	0.63	32
$[Co_4(SPh)_{10}]^{2-}$, Co_4	4740	643	0.65	32
Co^{2+}:CdS	3160	664	0.67	33

All energies are in cm^{-1}. [a]Nephelauxetic ratio, $\beta = B_c/B_0$. Free-ion B value for Co^{2+} is $B_0 = 989\ cm^{-1}$.[34]

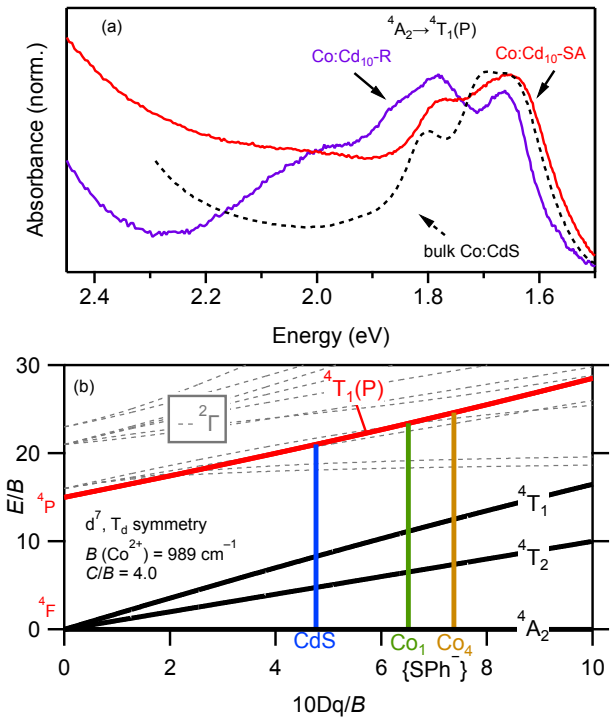

Figure 5. (a) Normalized electronic absorption spectra of the $^4A_2 \rightarrow {}^4T_1(P)$ transition from $(Cd_{0.9}Co_{0.1})_{10}$-SA compared with $(Cd_{0.9}Co_{0.1})_{10}$-R and colloidal Co:CdS nanocrystals grown from an iso-crystalline core/shell method reproduced from reference [35]. Copyright 2001 American Chemical Society. (b) Tanabe-Sugano diagram for Co^{2+} in T_d symmetry showing spin-allowed (solid lines) and spin-forbidden transitions (dashed lines) with the observed excited state is shown in red. Vertical lines depict the estimated ligand field strengths for Co^{2+} in CdS (blue), $[Co(SPh)_4]^{2-}$ (Co_1, green), and $[Co_4(SPh)_{10}]^{2-}$ (Co_4, brown) using the data in Table 1.

The Cd_{10} clusters readily form single crystals under certain recrystallization conditions.[9,39,40] We were unable to obtain crystals suitable for single-crystal studies from the Co:Cd_{10}-SA synthesis, however the formation of single crystals using various counter ions is currently under investigation. We were instead able to examine the structure by powder X-ray diffraction of the prepared powders, shown in Figure 6a. Additionally, the powders of the Cd_{10}-R clusters were prepared by the precipitation from diethyl ether. The diffraction patterns of the Co:Cd_{10}-SA powders display the many expected narrow peaks of the Cd_{10} clusters that crystallize primarily in the $P\bar{4}2_{1/c}$ space group[39,40] with Me_4N^+ counterions. We also observe the $I\bar{4}$ space group[9] as a minority phase presumably due to the nature of the isolation and precipitation procedure that may lead to the presence of multiple crystalline phases. While the patterns match relatively well, there is a notable absence of the broad peaks centered around 28° and 48° 2θ for the Cd_{10}-R powders. While it is commonly known that small nanocrystals tend to have broad peaks in XRD due to their small crystallite size, it has also been shown that amorphous Cd_{10} frameworks and clusters of larger nuclearity display similar broad features in the same regions.[6,36] However, the solution electronic absorption spectra above favors the assignment to Cd_{20} or other large cluster species prepared from the self-assembly method. As the dopant concentration in the Co:Cd_{10}-SA cluster increases, there is a clear shift of the (110) and (101) peaks to larger 2θ values. This observation is consistent with substitution of the smaller Co^{2+} ion into the larger Cd^{2+} host site, however, the PXRD results do not allow us to resolve the distribution or site occupancy of Co^{2+} in the Cd_{10}-SA cluster.

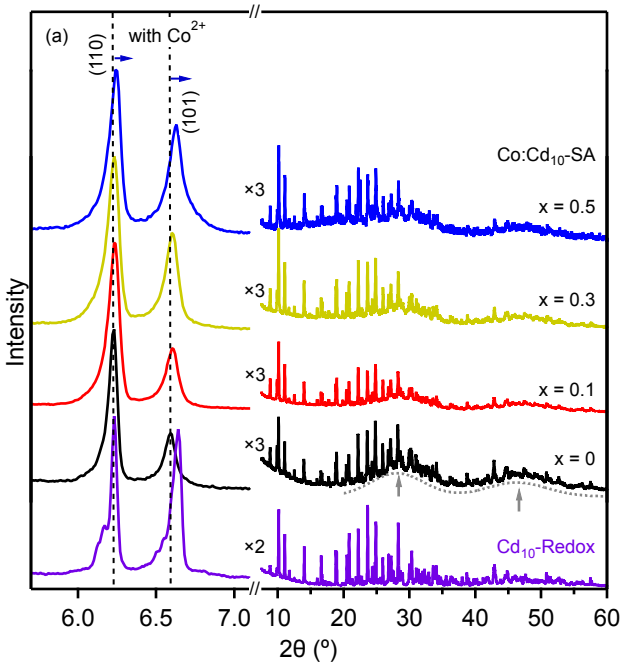

Figure 6. Powder XRD of the $(Cd_{1-x}Co_x)_{10}$-SA clusters with x = 0, 0.1, 0.3, and 0.5, and Cd_{10}-R. The relative intensities of the peaks between 7.5° < 2θ < 60° are scaled by 3 for closer inspection. Broad features are observed at ca. 28° and 48° in all the SA clusters as shown by the dotted line near the x = 0 pattern that was produced by fitting the pattern to two Gaussian functions.

We previously demonstrated the site-selective incorporation of Mn^{2+} dopants within the Cd_{10}-SA core, however, over time the Mn^{2+} dopant would leave the cores as evidenced by photoluminescence spectroscopy.[29] We did not observe any change in the electronic absorption spectra or ESI-MS of the Co:Cd_{10}-SA clusters. The difference in stability between Mn^{2+} and Co^{2+} within the Cd_{10} core sites could originate from the relative hardness of these cations with S^{2-} and SPh^-. These hard-soft acid-base (HSAB) considerations predict that hard acids such as Mn^{2+} prefer the ligand field environment of the precursor nitrate or water while borderline acids such as Co^{2+} prefer sulfide ligands within the Cd_{10} core. This simple HSAB approach to rationalizing dopant stability in clusters could be extended to different host lattices such as Zn_{10} or in clusters with substituted 4-R-SPh^- ligands where the R group can be modified to make the thiophenolate ligand harder or softer. These studies are currently underway.

CONCLUSIONS

The use of this self-assembly synthetic method, combined with the varying ratio of Cd^{2+} to Co^{2+}, allows for the preparation of heavily-doped Cd_{10} clusters. This approach circumvents the thermodynamic barrier associated with core doping to pre-formed Cd_{10}-R clusters. Maintaining the Cd^{2+}:Co^{2+} ratio during the self-assembly synthesis shows that Co^{2+} acts can substitute for Cd^{2+} at both surface and core sites, which we hypothesize is the result of the cluster equilibrium favoring Cd_{10} formation compared to Cd_8 and Cd_{17} formation. In contrast, Co:Cd_{10}-R clusters only result in surface substitution. We further strengthened the ESI-MS conclusion of variations in the Co^{2+} doping sites between the Co:Cd_{10}-SA and Co:Cd_{10}-R

clusters by comparison of the electronic absorption spectra of the Co^{2+}-centered ligand field transition in the visible region. Studying these nanoclusters has provided some key insights to the mechanisms of cluster conversion and dopant incorporation that may also be relevant to analogous nanomaterials such as magic-size nanoclusters, ultrasmall nanocrystals, and colloidal semiconductor nanocrystals. Given the enhanced stability of Co^{2+} dopants and ability to obtain core doping, these Co:Cd_{10} clusters have the potential to act as true single-source precursors for achieving homogenously doped QDs and related nanomaterials.

ASSOCIATED CONTENT

Supporting Information

The Supporting Information is available free of charge on the ACS Publications website.

Additional synthetic details, ESI mass spectra, ESI-MS analysis and corresponding tables, and ICP-OES data (PDF).

AUTHOR INFORMATION

Corresponding Author

*e-mail: kittilstved@chem.umass.edu

Author Contributions

The manuscript was written through contributions of all authors.

Funding Sources

National Science Foundation: CHE-1454930

ACKNOWLEDGMENT

This work was supported by the National Science Foundation (Grant CHE-1454930). Mass spectra were obtained at the University of Massachusetts Mass Spectrometry Center. Powder X-ray diffraction data was collected with assistance from Haneen Mansoor and made possible through the National Science Foundation Major Research Instrumentation Program (Grant CHE-1726578). We thank Dr. Fumitoshi Kato and Dr. Swamy Pittala for valuable discussions and insight at the early stages of this project.

REFERENCES

(1) Beecher, A. N.; Yang, X.; Palmer, J. H.; LaGrassa, A. L.; Juhas, P.; Billinge, S. J. L.; Owen, J. S. Atomic Structures and Gram Scale Synthesis of Three Tetrahedral Quantum Dots. *J. Am. Chem. Soc.* **2014**, *136*, 10645–10653.

(2) Corrigan, J. F.; Fuhr, O.; Fenske, D. Metal Chalcogenide Clusters on the Border between Molecules and Materials. *Advanced Materials* **2009**, *21*, 1867–1871.

(3) Soloviev, V. N.; Eichhöfer, A.; Fenske, D.; Banin, U. Size-Dependent Optical Spectroscopy of a Homologous Series of CdSe Cluster Molecules. *J. Am. Chem. Soc.* **2001**, *123*, 2354–2364.

(4) Alivisatos, A. P. Semiconductor Clusters, Nanocrystals, and Quantum Dots. *Science* **1996**, *271*, 933–937.

(5) Soloviev, V. N.; Eichhöfer, A.; Fenske, D.; Banin, U. Molecular Limit of a Bulk Semiconductor: Size Dependence of the "Band Gap" in CdSe Cluster Molecules. *J. Am. Chem. Soc.* **2000**, *122*, 2673–2674.

(6) Levchenko, T. I.; Lucier, B. E. G.; Corrigan, J. F.; Huang, Y. Crystalline Superlattices of Nanoscopic CdS Molecular Clusters: An X-Ray Crystallography and ^{111}Cd SSNMR Spectroscopy Study. *Inorg. Chem.* **2018**, *57*, 204–217.

(7) Hsieh, T.-E.; Yang, T.-W.; Hsieh, C.-Y.; Huang, S.-J.; Yeh, Y.-Q.; Chen, C.-H.; Li, E. Y.; Liu, Y.-H. Unraveling the Structure of Magic-Size $(CdSe)_{13}$ Cluster Pairs. *Chem. Mater.* **2018**, *30*, 5468–5477.

(8) Turk, T.; Resch, U.; Fox, M. A.; Vogler, A. Cadmium Benzenethiolate Clusters of Various Size: Molecular Models for Metal Chalcogenide Semiconductors. *J. Phys. Chem.* **1992**, *96*, 3818–3822.

(9) Dance, I. G.; Choy, A.; Scudder, M. L. Syntheses, Properties, and Molecular and Crystal Structures of $(NMe_4)_4[E_4M_{10}(SPh)_{16}]^{4-}$ (E = Sulfur or Selenium; M = Zinc or Cadmium): Molecular Supertetrahedral Fragments of the Cubic Metal Chalcogenide Lattice. *J. Am. Chem. Soc.* **1984**, *106*, 6285–6295.

(10) Choy, A.; Craig, D.; Dance, I.; Scudder, M. $[S_4Cd_{10}(SPh)_{16}]^{4-}$ (M=Zn, Cd), a Molecular Fragment of the Sphalerite Ms Lattice: Structural Congruence of Metal Sulphides and Metal Thiolates. *J. Chem. Soc., Chem. Commun.* **1982**, 1246–1247.

(11) Eichhöfer, A.; Hampe, O.; Blom, M. Synthesis, Structures, and Properties of a Series of $[Cd_8Se(SePh)_{12}Cl_4]^{2-}$ Cluster Compounds with Different Counterions. *European Journal of Inorganic Chemistry* **2003**, 1307–1314.

(12) Lee, G. S. H.; Craig, D. C.; Ma, Ida.; Scudder, M. L.; Bailey, T. D.; Dance, I. G. $[S_4Cd_{17}(SPh)_{28}]^{2-}$, the First Member of a Third Series of Tetrahedral $[S_WM_X(SR)_Y]^{z-}$ Clusters. *J. Am. Chem. Soc.* **1988**, *110*, 4863–4864.

(13) Herron, N.; Calabrese, J. C.; Farneth, W. E.; Wang, Y. Crystal Structure and Optical Properties of $Cd_{32}S_{14}(SC_6H_5)_{36}\bullet DMF_4$, a Cluster with a 15 Angstrom CdS Core. *Science* **1993**, *259*, 1426–1428.

(14) Friedfeld, M. R.; Johnson, D. A.; Cossairt, B. M. Conversion of InP Clusters to Quantum Dots. *Inorg. Chem.* **2019**, *58*, 803–810.

(15) Jiang, Z.-J.; Kelley, D. F. Role of Magic-Sized Clusters in the Synthesis of CdSe Nanorods. *ACS Nano* **2010**, *4*, 1561–1572.

(16) Cumberland, S. L.; Hanif, K. M.; Javier, A.; Khitrov, G. A.; Strouse, G. F.; Woessner, S. M.; Yun, C. S. Inorganic Clusters as Single-Source Precursors for Preparation of CdSe, ZnSe, and CdSe/ZnS Nanomaterials. *Chem. Mater.* **2002**, *14*, 1576–1584.

(17) Fregnaux, M.; Arl, D.; Dalmasso, S.; Gaumet, J.-J.; Laurenti, J.-P. Physical and Chemical Analyses on Single-Source Precursor-Grown CdS Semiconductor Nanomaterials. *J. Phys. Chem. C* **2010**, *114*, 17318–17323.

(18) Bendova, M.; Puchberger, M.; Pabisch, S.; Peterlik, H.; Schubert, U. Studies on the Formation of CdS Nanoparticles from Solutions of $(NMe_4)_4[S_4Cd_{10}(SPh)_{16}]^{4+}$. *European Journal of Inorganic Chemistry* **2010**, 2266–2275.

(19) Archer, P. I.; Santangelo, S. A.; Gamelin, D. R. Inorganic Cluster Syntheses of TM^{2+}-Doped Quantum Dots (CdSe, CdS, CdSe/CdS): Physical Property Dependence on Dopant Locale. *J. Am. Chem. Soc.* **2007**, *129*, 9808–9818.

(20) Hanif, K. M.; Meulenberg, R. W.; Strouse, G. F. Magnetic Ordering in Doped Cd1-XCoxSe Diluted Magnetic Quantum Dots. *J. Am. Chem. Soc.* **2002**, *124*, 11495–11502.

(21) Cossairt, B. M.; Owen, J. S. CdSe Clusters: At the Interface of Small Molecules and Quantum Dots. *Chem. Mater.* **2011**, *23*, 3114–3119.

(22) Friedfeld, M. R.; Stein, J. L.; Cossairt, B. M. Main-Group-Semiconductor Cluster Molecules as Synthetic Intermediates to Nanostructures. *Inorg. Chem.* **2017**, *56*, 8689–8697.

(23) Gary, D. C.; Terban, M. W.; Billinge, S. J. L.; Cossairt, B. M. Two-Step Nucleation and Growth of InP Quantum Dots via Magic-Sized Cluster Intermediates. *Chem. Mater.* **2015**, *27*, 1432–1441.

(24) Dagtepe, P.; Chikan, V.; Jasinski, J.; Leppert, V. J. Quantized Growth of CdTe Quantum Dots; Observation of Magic-Sized CdTe Quantum Dots. *J. Phys. Chem. C* **2007**, *111*, 14977–14983.

(25) Zhang, J.; Hao, X.; Rowell, N.; Kreouzis, T.; Han, S.; Fan, H.; Zhang, C.; Hu, C.; Zhang, M.; Yu, K. Individual Pathways in the Formation of Magic-Size Clusters and Conventional Quantum Dots. *J. Phys. Chem. Lett.* **2018**, *9*, 3660–3666.

(26) Pittala, S.; Mortelliti, M. J.; Kato, F.; Kittilstved, K. R. Substitution of Co^{2+} Ions into CdS-Based Molecular Clusters. *Chem. Commun.* **2015**, *51*, 17096–17099.

(27) Pittala, S.; Kittilstved, K. R. Cation Exchange in Small ZnS and CdS Molecular Analogues. *Inorg. Chem.* **2015**, *54*, 5757–5767.

(28) Zhang, J.; Bu, X.; Feng, P.; Wu, T. Metal Chalcogenide Supertetrahedral Clusters: Synthetic Control over Assembly, Dispersibility, and Their Functional Applications. *Acc. Chem. Res.* **2020**, *53*, 2261–2272.

(29) Kato, F.; Kittilstved, K. R. Site-Specific Doping of Mn^{2+} in a CdS-Based Molecular Cluster. *Chem. Mater.* **2018**, *30*, 4720–4727.

(30) Dance, I. G.; Calabrese, J. C. X-Ray Structure of the Hexa(μ_2-Arenethiolato-)Tetra(Arenethiolato)Tetracobaltate(II) Dianion, $[(Co\text{-}SPh)_4(\mu_2\text{-}SPh)_6]^{2-}$, a New Tetrahedral Tetracobalt Thiolate Cluster. *J. Chem. Soc., Chem. Commun.* **1975**, No. 18, 762–763.

(31) Bryan, J. D.; Gamelin, D. R. Doped Semiconductor Nanocrystals: Synthesis, Characterization, Physical Properties, and Applications. In *Progress in Inorganic Chemistry*; John Wiley & Sons, Ltd, 2005; pp 47–126.

(32) Nakata, M.; Ueyama, N.; Nakamura, A.; Nozawa, T.; Hatano, M. Circular Dichroism and Magnetic Circular Dichroism Spectra of Tetrahedral Cobalt(II) Complexes of Thiophenolate, o-Xylene-.Alpha.,.Alpha.'-Dithiolate, and L-Cysteine-Containing Oligopeptides. *Inorg. Chem.* **1983**, *22*, 3028–3035.

(33) Pappalardo, R.; Dietz, R. E. Absorption Spectra of Transition Ions in CdS Crystals. *Phys. Rev.* **1961**, *123*, 1188–1203.

(34) Brorson, M.; Schaeffer, C. E. Orthonormal Interelectronic Repulsion Operators in the Parametrical Dq Model. Application of the Model to Gaseous Ions. *Inorg. Chem.* **1988**, *27*, 2522–2530.

(35) Radovanovic, P. V.; Gamelin, D. R. Electronic Absorption Spectroscopy of Cobalt Ions in Diluted Magnetic Semiconductor Quantum Dots: Demonstration of an Isocrystalline Core/Shell Synthetic Method. *J. Am. Chem. Soc.* **2001**, *123*, 12207–12214.

(36) Herron, N.; Suna, A.; Wang, Y. A Synthesis of ~10 Å Thiophenolate-Capped CdS Clusters. Observation of a Sharp Absorption Peak. *J. Chem. Soc., Dalton Trans.*, 2329–2335.

(37) Schwartz, D. A.; Norberg, N. S.; Nguyen, Q. P.; Parker, J. M.; Gamelin, D. R. Magnetic Quantum Dots: Synthesis, Spectroscopy, and Magnetism of Co^{2+}- and Ni^{2+}-Doped ZnO Nanocrystals. *J. Am. Chem. Soc.* **2003**, *125*, 13205–13218.

(38) Dance, I. G. Synthesis, Crystal Structure, and Properties of the Hexa(μ-Benzenethiolato)Tetra(Benzenethiolatocobaltate(II)) Dianion, the Prototype Cobalt(II)-Thiolate Molecular Cluster. *J. Am. Chem. Soc.* **1979**, *101*, 6264–6273.

(39) Lee, G. S. H.; Fisher, K. J.; Vassallo, A. M.; Hanna, J. V.; Dance, I. G. Solid-State ^{113}Cd NMR of Three Structural Isomers of $[S_4Cd_{10}(SPh)_{16}]^{4-}$. *Inorg. Chem.* **1993**, *32*, 66–72.

(40) Adams, R.; Zhang, B.; J. Murphy, C.; K. Yeung, L. Halide Enhancement of the Luminescence of $Cd_{10}S_4$ Thiolate Clusters. *Chem. Commun.* **1999**, *4*, 383–384.

TOC GRAPHIC

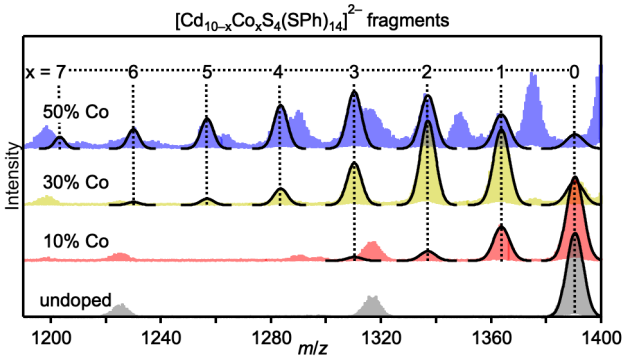

Synopsis. The successful doping of up to seven cobalt ions into decameric cadmium sulfide thiophenolate clusters by a self-assembly synthetic method is demonstrated. This finding requires at least one cobalt ion to be located within the core site of the cluster. These clusters are stable and provide a promising step towards understanding the solution chemistry and assembly mechanism of these molecular analogs of semiconductor nanocrystals.

Supporting Information to

Core Doped $[(Cd_{1-x}Co_x)_{10}S_4(SPh)_{16}]^{4-}$ Clusters from a Self-Assembly Route

Jillian E. Denhardt and Kevin R. Kittilstved*

Department of Chemistry, University of Massachusetts Amherst, 710 N Pleasant St, Amherst, MA 01003

*email – kittilstved@chem.umass.edu

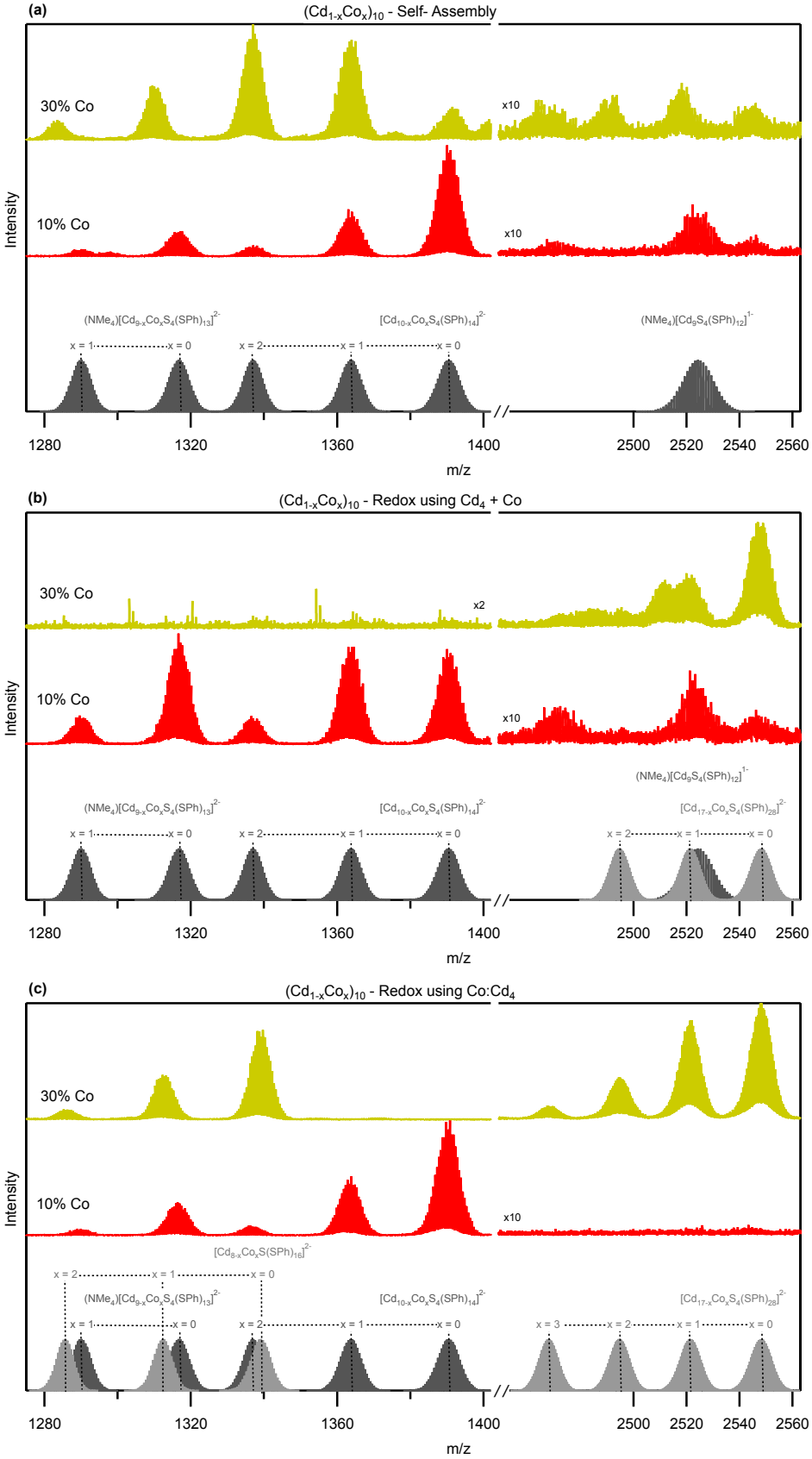

Figure S1. Comparison of the Co:Cd_{10}-SA (a) and Co:Cd_{10}-R (b and c) method products by ESI-MS. (b) At dopant concentrations of even 30% Co^{2+}, the Co:Cd_{10}-R shows no Cd_{10} synthesis and instead shows the apparent formation of Cd_{17}. Observation of a precipitate during the addition of the Co^{2+} during synthesis also indicates a disruption in the Cd_{10} formation. This result demonstrates that high-doping levels initiates cluster growth instead of maintaining simple metal-ion equilibria between cations in Cd_{10} and solution. (c) However, when a pre-doped Co:Cd_4 cluster was used as the precursor for the redox method, which would maintain the S^{2-}:TM^{2+} ratio even at higher dopant concentrations similarly to the SA method, the formation of Co^{2+} doped Cd_8 and Cd_{17} is instead observed at 30% Co^{2+}.

Table S1. Abbreviated list of ESI-MS peaks for Co:Cd_{10}-R Clusters

Observed Fragments from Co:Cd10-R Syntheses	m/z (calc)	m/z (exp)	Relative Peak Height (%) of Fragments				
				from Undoped Cd_4 + Co		from Co:Cd_4	
			Undoped	10%	30%	10%	30%
$[Cd_{17}S_4(SPh)_{28}]^{2-}$	2548	2548	0.0	0.0	100.0	0.0	100.0
$[Cd_{16}Co_1S_4(SPh)_{28}]^{2-}$	2521	2521			47.7		85.2
$[Cd_{15}Co_2S_4(SPh)_{28}]^{2-}$	2494	2494			19.2		36.4
$[Cd_{14}Co_3S_4(SPh)_{28}]^{2-}$	2468	2468					11.4
$[Cd_{13}Co_4S_4(SPh)_{28}]^{2-}$	2411	2411					3.8
$[Cd_{10}S_4(SPh)_{14}]^{2-}$	1390	1390	100.0	86.0	0.0	100.0	0.0
$[Cd_9Co_1S_4(SPh)_{14}]^{2-}$	1364	1364		87.7		51.2	
$[Cd_9Co_1S_4(SPh)_{14}]^{2-}$	1337	1337		26.1		8.6	
$(NMe_4)[Cd_9S_4(SPh)_{13}]^{2-}$	1317	1317	19.4	100.0	0.0	28.6	0.0
$(NMe_4)[Cd_8Co_1S_4(SPh)_{13}]^{2-}$	1290	1290		26.5		6.1	
$[Cd_8S_1(SPh)_{16}]^{2-}$	1339	1339	0.0	0.0	0.0	0.0	77.1
$[Cd_7Co_1S_1(SPh)_{16}]^{2-}$	1312	1312					38.4
$[Cd_6Co_2S_1(SPh)_{16}]^{2-}$	1285	1285					8.6
$[Cd_5Co_3S_1(SPh)_{16}]^{2-}$	1259	1259					1.4

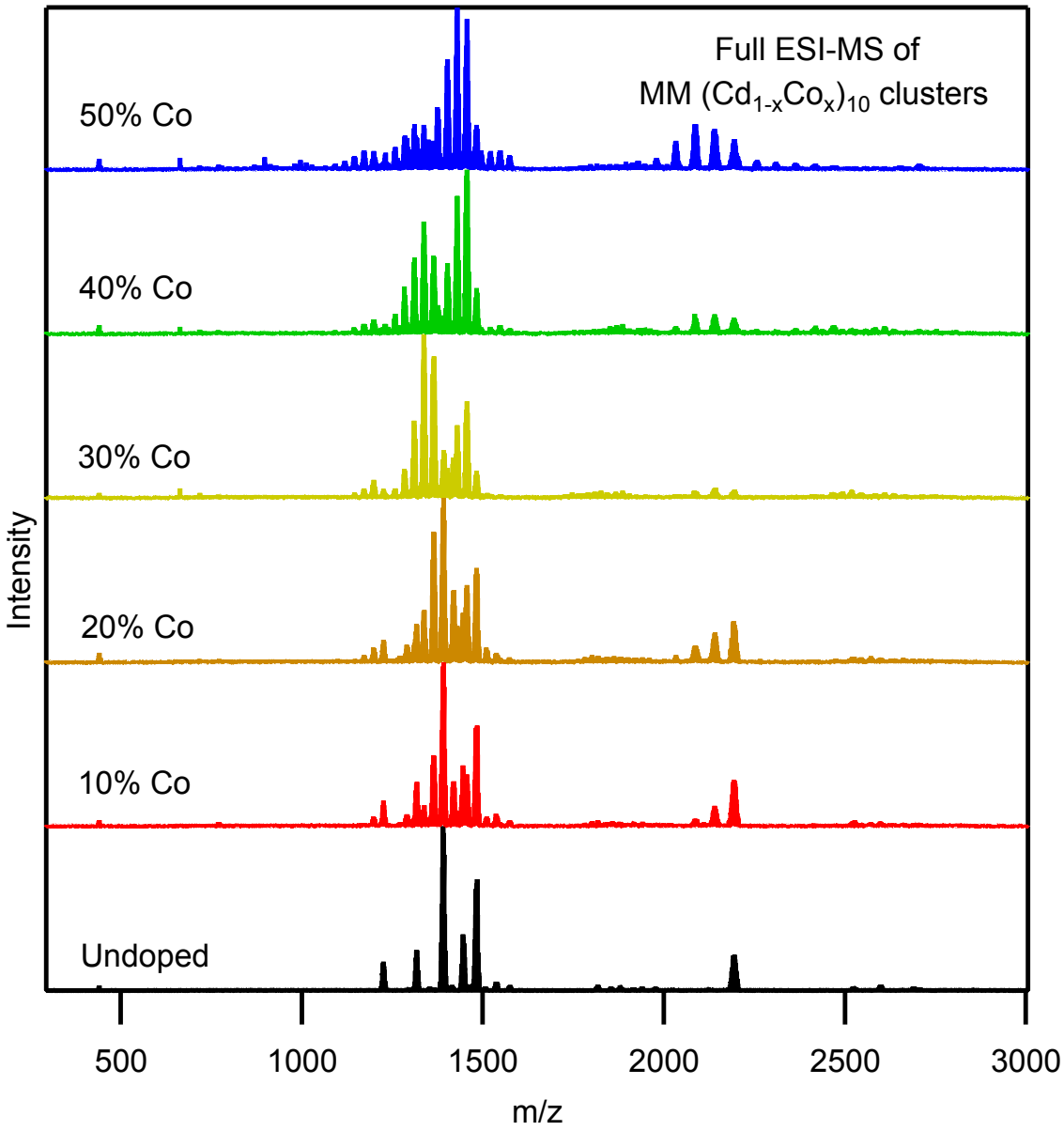

Figure S2. Full ESI-MS spectra for the $(Cd_{1-x}Co_x)_{10}$-SA samples at different dopant concentrations of x= 0 to 0.5.

Table S2. ESI-MS peaks for Co:Cd_{10}-SA Clusters

$(NMe_4)_2[(Cd_{1-x}Co_x)_{10}S_4(SPh)_{16}]$ Observed Fragments	m/z (calc)	m/z (exp)	Relative Peak Height (%) of fragments Undoped	10% Co	30% Co	50% Co
$(NMe_4)[Cd_8S_4(SPh)_{10}]^{1-}$	2194	2194	21.8	29.2	5.0	18.8
$(NMe_4)[Cd_7Co_1S_4(SPh)_{10}]^{1-}$	2139	2139		13.0	6.0	24.7
$(NMe_4)[Cd_6Co_2S_4(SPh)_{10}]^{1-}$	2086	2086		3.4	4.0	28.2
$(NMe_4)[Cd_5Co_3S_4(SPh)_{10}]^{1-}$	2033	2033			2.0	17.9
$(NMe_4)[Cd_4Co_4S_4(SPh)_{10}]^{1-}$	1979	1979				7.3
$(NMe_4)_2[Cd_{10}S_4(SPh)_{16}]^{2-}$	1574	1574	3.2	2.8	1.1	8.5
$(NMe_4)_2[Cd_9Co_1S_4(SPh)_{16}]^{2-}$	1547	1547		1.8	1.9	12.1
$(NMe_4)_2[Cd_8Co_2S_4(SPh)_{16}]^{2-}$	1520	1520			2.0	11.0
$(NMe_4)_2[Cd_7Co_3S_4(SPh)_{16}]^{2-}$	1493	1493			1.6	10.4
$(NMe_4)_2[Cd_6Co_5S_4(SPh)_{16}]^{2-}$	1467	1467				9.9
$(NMe_4)_2[Cd_{10}S_4(SPh)_{15}Cl]^{2-}$	1537	1537	4.6	6.2	1.1	2.3
$(NMe_4)_2[Cd_9Co_1S_4(SPh)_{15}Cl]^{2-}$	1510	1510		5.6	2.1	2.7
$(NMe_4)[Cd_{10}S_4(SPh)_{15}]^{2-}$	1482	1482	65.0	58.7	13.8	27.5
$(NMe_4)[Cd_9Co_1S_4(SPh)_{15}]^{2-}$	1455	1455		32.3	55.2	93.0
$(NMe_4)[Cd_8Co_2S_4(SPh)_{15}]^{2-}$	1428	1428		9.5	44.5	100.0
$(NMe_4)[Cd_7Co_3S_4(SPh)_{15}]^{2-}$	1401	1401			18.3	68.2
$(NMe_4)[Cd_6Co_4S_4(SPh)_{15}]^{2-}$	1375	1375			7.4	38.6
$(NMe_4)[Cd_5Co_5S_4(SPh)_{15}]^{2-}$	1348	1348				17.8
$(NMe_4)[Cd_{10}S_4(SPh)_{14}Cl]^{2-}$	1445	1445	34.4	35.5	4.7	7.9
$(NMe_4)[Cd_9Co_1S_4(SPh)_{14}Cl]^{2-}$	1418	1418		28.3	24.7	7.5
$[Cd_{10}S_4(SPh)_{14}]^{2-}$	1390	1390	100.0	100.0	26.0	7.8
$[Cd_9Co_1S_4(SPh)_{14}]^{2-}$	1364	1364		44.5	86.6	16.8
$[Cd_8Co_2S_4(SPh)_{14}]^{2-}$	1337	1337		10.3	100.0	25.5
$[Cd_7Co_3S_4(SPh)_{14}]^{2-}$	1310	1310			47.1	28.2
$[Cd_6Co_4S_4(SPh)_{14}]^{2-}$	1283	1283			17.6	20.9
$[Cd_5Co_5S_4(SPh)_{14}]^{2-}$	1257	1257			5.7	13.9
$[Cd_4Co_6S_4(SPh)_{14}]^{2-}$	1230	1230				10.3
$[Cd_3Co_7S_4(SPh)_{14}]^{2-}$	1203	1203				6.3
$[Cd_{10}S_4(SPh)_{13}Cl]^{2-}$	1353	1353	1.9	5.3	4.0	
$(NMe_4)[Cd_9S_4(SPh)_{13}]^{2-}$	1317	1317	24.4	26.2	4.8	20.1
$(NMe_4)[Cd_8Co_1S_4(SPh)_{13}]^{2-}$	1290	1290		7.4	4.4	19.6
$(NMe_4)[Cd_7Co_2S_4(SPh)_{13}]^{2-}$	1263	1263			1.6	7.4
$(NMe_4)[Cd_6Co_3S_4(SPh)_{13}]^{2-}$	1236	1236				4.3
$[Cd_9S_4(SPh)_{12}]^{2-}$	1225	1225	17.5	15.9	5.6	5.3
$[Cd_8Co_1S_4(SPh)_{12}]^{2-}$	1198	1198		5.4	5.1	11.7
$[Cd_7Co_2S_4(SPh)_{12}]^{2-}$	1171	1171		1.8	2.9	11.8
$[Cd_6Co_3S_4(SPh)_{12}]^{2-}$	1145	1145				8.6
Unobserved Fragments						
$[Cd_8S_1(SPh)_{15}]^{1-}$	2569					
$[Cd_{17}S_4(SPh)_{28}]^{2-}$	2548					
$(NMe_4)[Cd_4(SPh)_{10}]^{1-}$	1616					
$[Cd_4(SPh)_9]^{1-}$	1432					
$[Cd_8S_1(SPh)_{16}]^{2-}$	1339					
$[Cd_4(SPh)_{10}]^{2-}$	771					

Table S3. Precursor amounts and stoichiometric ratios used in the self-assembly and redox syntheses (units in mmol).

	Cd^{2+}	Co^{2+}	$Cd^{2+}+Co^{2+}$	PhS^{-}	S or S^{2-}	$PhS^{-}:TM^{2+}$	$S:TM^{2+}$	$PhS^{-}:S$ or $PhS^{-}:S^{2-}$
Undoped Cd_{10}-SA	2.38	0.0	2.38	5.20	1.20	2.18	0.504	4.33
10% $Co:Cd_{10}$-SA	2.14	0.238	2.38	5.20	1.20	2.18	0.504	4.33
30% $Co:Cd_{10}$-SA	1.67	0.714	2.38	5.20	1.20	2.18	0.504	4.33
Undoped Cd_{10}-R	2.37	0.0	2.37	5.92	0.624	2.50	0.263	9.49
10% $Co:Cd_{10}$-R	2.37	0.264	2.63	5.92	0.624	2.25	0.237	9.49
30% $Co:Cd_{10}$-R	2.37	1.01	3.38	5.92	0.624	1.75	0.184	9.49

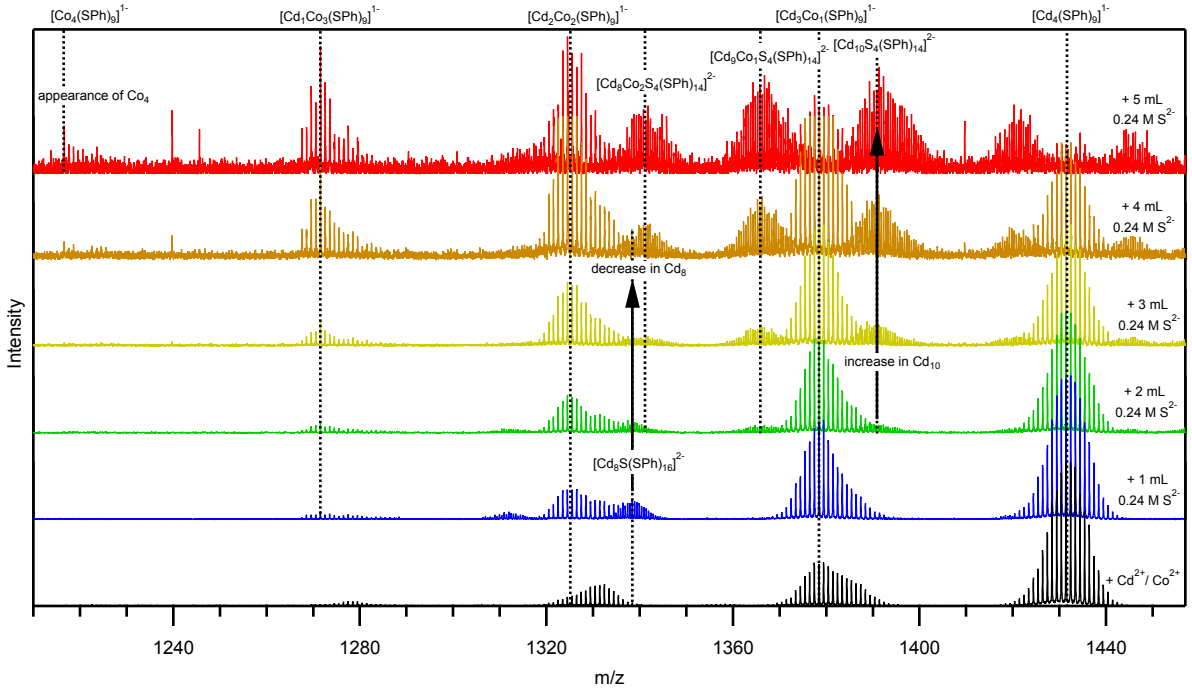

Figure S3. ESI-MS of reaction aliquots taken during the synthesis of 10% $Co:Cd_{10}$-SA with increasing amount of the S^{2-} precursor being added. The initial addition of the TM^{2+} precursor to the PHS- shows the formation of $Co:Cd_4$ by the observation of the $[Cd_{4-x}Co_x(SPh)_9]^{1-}$ fragment, which exists and shows a relative increase in the Co^{2+} dominated fragments as the reaction proceeds, including the formation of the Co_4 cluster once all the S^{2-} has been added. This shows the formation of Co_4 does not inhibit the $Co:Cd_{10}$ formation. Upon the addition of S^{2-}, the Cd_8 cluster is formed, observed by the $[Cd_8S(SPh)_{16}]^{2-}$ fragment, then decreases in relative intensity as S^{2-} is added while $Co:Cd_{10}$ forms, observed by the $[Cd_{10-x}Co_xS_4(SPh)_{14}]^{2-}$ fragment, and increases in relative intensity.

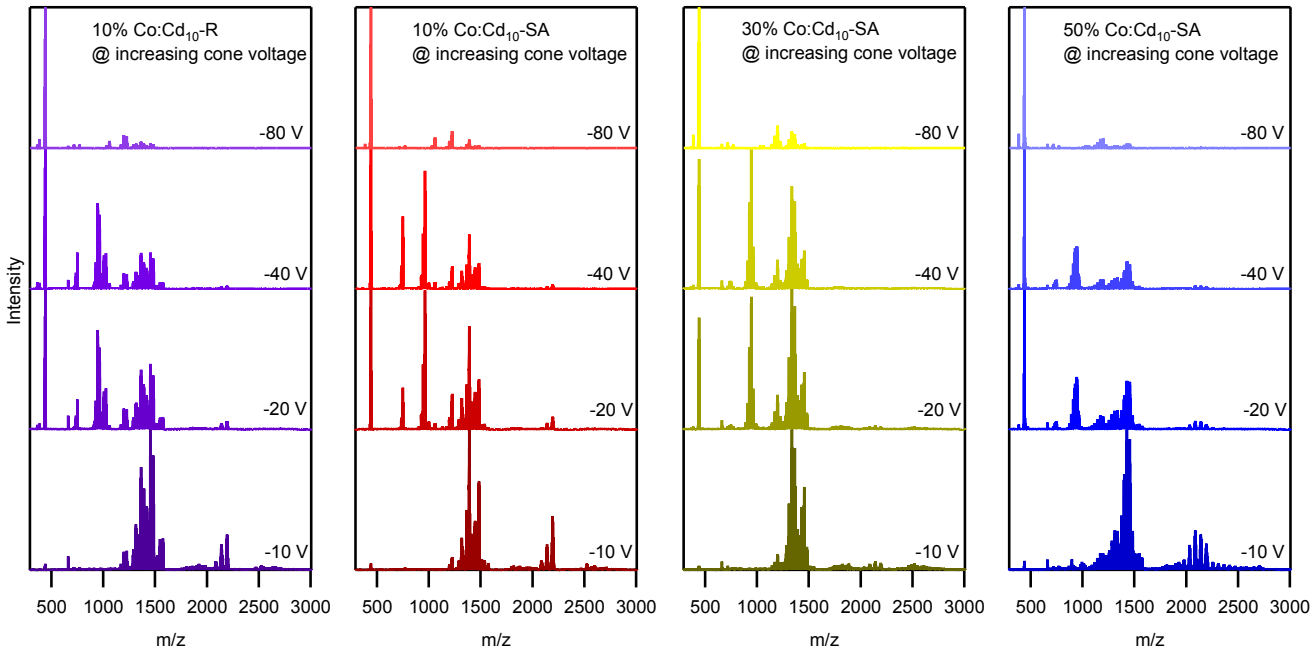

Figure S4. Full ESI-MS spectra of $(Cd_{0.9}Co_{0.1})_{10}$-R and $(Cd_{1-x}Co_x)_{10}$-SA for $x = 0.1 - 0.5$ measured at higher cone voltages, ranging from −10 V to −80 V.

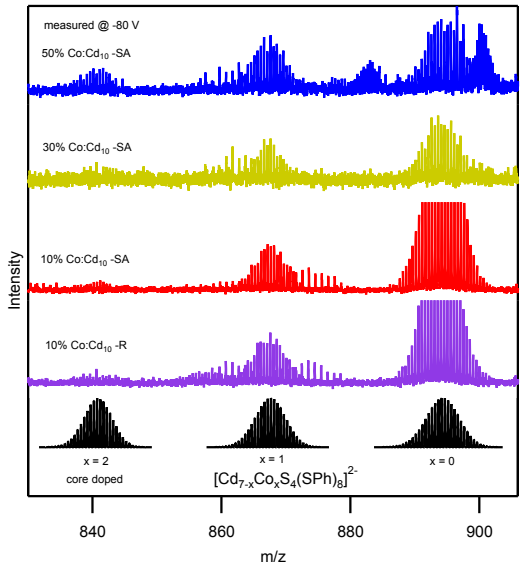

Figure S5. ESI-MS of $(Cd_{0.9}Co_{0.1})_{10}$-R and $(Cd_{1-x}Co_x)_{10}$-SA for $x = 0.1 - 0.5$ measured at −80 V to observe the $[Cd_{7-x}Co_xS_4(SPh)_8]^{2-}$ fragment with up to 2 Co^{2+} ions that must include one dopant occupying a core site. While at low dopant concentrations of 10% Co^{2+} for Cd_{10}-SA and Cd_{10}-R, core doping cannot be discerned, but at 50% Co^{2+} core doping can be clearly observed in the Co:Cd_{10}-SA cluster.

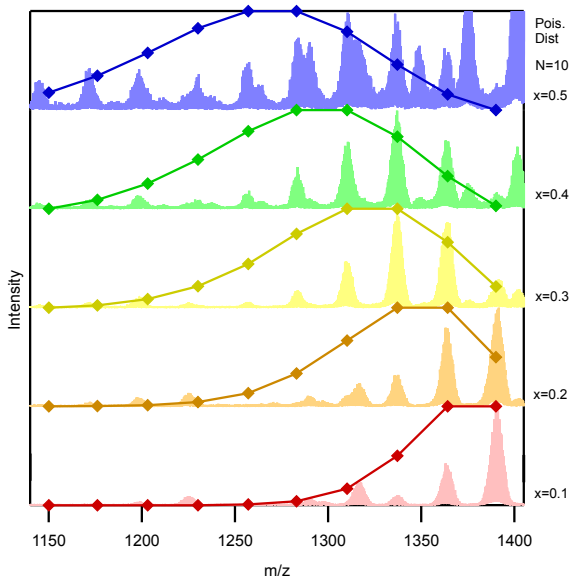

Figure S6. The calculated values for the Poissonian distribution as compared to the ESI-MS spectra for $(Cd_{1-x}Co_x)_{10}$-SA for $x = 0.1 - 0.5$.

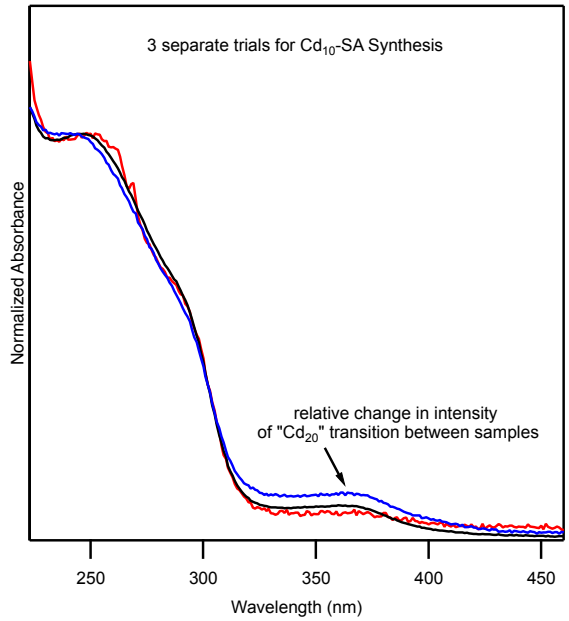

Figure S7. Electronic absorption for multiple batches of undoped Cd_{10}-SA shows the relative intensity of the tentatively assigned "Cd_{20}" transition changes as compared to the intensity of the Cd_{10} intraligand transition, supporting the hypothesis of their being two separate species.

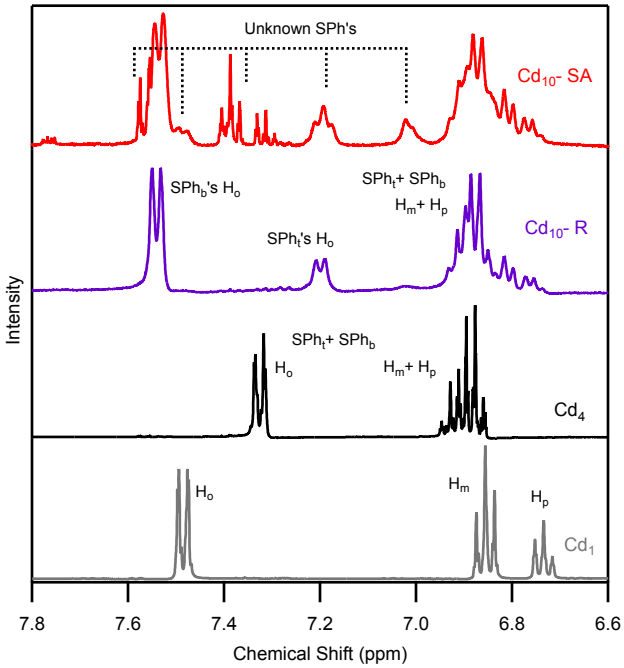

Figure S8. ^{1}H NMR of the two different Cd_{10} samples, R and SA, along with $(NMe_4)_2[Cd(SPh)_4]$ and $(NMe_4)_2[Cd_4(SPh)_{10}]$ clusters shows the bridging (SPh_b) and terminal (SPh_t) thiophenolate protons to display the differences between the clusters. While these protons can be discerned in the Cd_{10}-R, there are two additional sets of unknown thiophenolate peaks in the Cd_{10}-SA. This demonstrates the ability to observe additional clusters within the solution and possibly provides evidence for the existence of the "Cd_{20}" cluster.

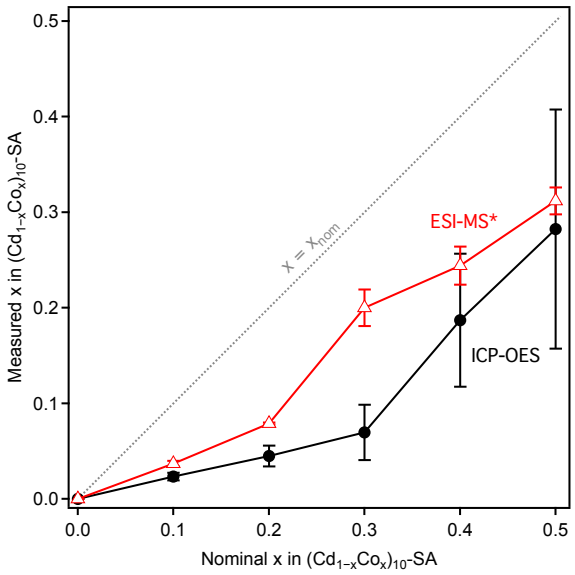

Figure S9. Dopant concentration, *x*, measured by ICP-OES (black closed circles) and the ESI-MS Poissonian fitting analysis of the $[(Cd_{10-x}Co_x)S_4(SPh)_{14}]^{2-}$ product fragments (red open triangles) as a function of the nominal dopant concentration used in the synthesis of the Co:Cd_{10}-SA clusters.